nanomaterials

MDPI

Article

Direct Fabrication of $CsPb_xMn_{1-x}(Br,Cl)_3$ Thin Film by a Facile Solution Spraying Approach

Yu Sun [1,2], Jin Chen [1,*], Fengchao Wang [1,*], Yi Yin [1], Yan Jin [1,2], Jun Wang [1], Xiaogai Peng [3], Ruiyi Han [1], Canyun Zhang [1], Jinfang Kong [1] and Jing Yang [1]

[1] Shanghai Institute of Technology, College of Sciences, 100 Haiquan Road, Shanghai 201418, China; yusunwei@126.com (Y.S.); particularlymin@outlook.com (Y.Y.); jinyan@sit.edu.cn (Y.J.); wangj@sit.edu.cn (J.W.); ruiyihan39@163.com (R.H.); zhang_canyun@sit.edu.cn (C.Z.); jfkong@sit.edu.cn (J.K.); yangjingxqq@sit.edu.cn (J.Y.)

[2] State Key Laboratory of Transducer Technology, Shanghai Institute of Microsystem and Information Technology, Chinese Academy of Sciences, Shanghai 200050, China

[3] State Key Laboratory of Precision Spectroscopy, School of Physics and Electronic Science, East China Normal University, Shanghai 200062, China; pengxiaogai@163.com

* Correspondence: jinchenxl@sit.edu.cn (J.C.); fcwang@sit.edu.cn (F.W.); Tel.: +86-21-6087-3193 (J.C.)

Abstract: Nowadays, Mn-doping is considered as a promising dissolution for the heavy usage of toxic lead in $CsPbX_3$ perovskite material. Interestingly, Mn-doping also introduces an additional photoluminescence band, which is favorable to enrich the emission gamut of this cesium lead halide. Here, a solution spraying strategy was employed for the direct preparation of $CsPb_xMn_{1-x}(Br,Cl)_3$ film through $MnCl_2$ doping in host $CsPbBr_3$ material. The possible fabrication mechanism of the provided approach and the dependences of material properties on Mn-doping were investigated in detail. As the results shown, Pb was partially substituted by Mn as expected. With the ratio of $PbBr_2$:$MnCl_2$ increasing from 3:0 to 1:1, the obtained film separately featured green, cyan, orange-red and pink-red emission, which was caused by the energy transferring process. Moreover, the combining energy of Cs, Pb, and Mn gradually red-shifted resulted from the formation of Cs-Cl, Pb-Cl and Mn-Br coordination bonding as $MnCl_2$ doping increased. In addition, the weight of short decay lifetime of prepared samples increased with the doping rising, which indicated a better exciton emission and less defect-related transition. The aiming of current work is to provide a new possibility for the facile preparation of Mn-doping $CsPbX_3$ film material.

Keywords: $MnCl_2$ doping; $CsPb_xMn_{1-x}(Br,Cl)_3$; thin films; solution spraying

Citation: Sun, Y.; Chen, J.; Wang, F.; Yin, Y.; Jin, Y.; Wang, J.; Peng, X.; Han, R.; Zhang, C.; Kong, J.; et al. Direct Fabrication of $CsPb_xMn_{1-x}(Br,Cl)_3$ Thin Film by a Facile Solution Spraying Approach. *Nanomaterials* **2021**, *11*, 3242. https://doi.org/10.3390/nano11123242

Academic Editor: Efrat Lifshitz

Received: 8 October 2021
Accepted: 26 November 2021
Published: 29 November 2021

1. Introduction

All-inorganic $CsPbX_3$ (X=Cl, Br, or I) perovskite material has become a promising candidate for light emitting diodes (LEDs) [1], solar cells [2], lasers [3,4] and so forth [5,6] due to their superior optical properties [7], such as high color purity [8], high photoluminescence quantum yield (PLQY) [5], excellent carrier characteristics [9] and tunable band gap [10]. Unfortunately, the toxicity of lead is a great challenge for the development of lead halide perovskite [11,12]. How to reduce or replace lead by less-toxic or non-toxic metals is one of the key issues for its commercial application. Currently, great efforts have been made to partially or completely replace Pb by doping divalent cations (such as Sn^{2+}, Ge^{2+}, Zn^{2+}) as the core elements of $CsPbX_3$ material [13]. However, the susceptible oxidation of Sn and Ge from bivalent state to tetravalent state exposed under ambient environment is risky for the material stability. Regarding Zn^{2+}, the doping concentration in the host material is limited, which is unfavorable to further eliminate the toxic Pb use [14].

Interestingly, Mn-doped $CsPbX_3$ material has new pleasant chemical and physical properties. It has become a promising candidate for lead-less perovskite material [15]. As suggested by previous reports [16], Mn^{2+} doping can improve the material stability,

which derives from Mn-X bond having higher binding energy than Pb-X bond. The most interesting result after partial substitutions of Mn for Pb element is that there is an additional photoluminescence (PL) band in the orange region compared with the pure $CsPbX_3$ material [17,18]. Commonly, Mn-doped $CsPbX_3$ can be fabricated by halide exchange driven cation exchange strategy [19,20]. Sheldon and co-workers reported the first attempt at Mn-doping based on host material of $CsPbCl_3$ by hot injection method [17]. Later, Zhu et al. found that Mn also can doped into $CsPbBr_3$ structure via $MnCl_2$ to form mixed halide perovskites in 2017 [21]. These mixed halide perovskites can support a much higher Mn doping ratio while retaining the original perovskite emission [15,16,22]. Furthermore, Cl-to-Br anion exchange was adopted to modify the compositions of Mn-doped perovskite material, leading to multi-color luminescence [22]. It is known that the methods of hot injection [23], thermal solvent [24], and anti-solvent [20] are prevalent for the fabrication of Mn-doping $CsPbX_3$ material. However, these approaches are limited by the shortcomings of low yields, complex procedures, and toxic chemicals. In addition, the obtained product prepared by the above methods is in a powder-state rather than in film-state. It is well known that the solution spraying method is widely used for the multi-element material fabrication, such as ZnS [25], Cu_2SnS_3 [26], Cu_2ZnSnS_4 [27], etc., due to its prominent merits of low cost, simple operation, low time-consuming and scalable production. Yang et al. reported their work about the fabrication of $CsPbBr_3$ thin film through a spraying method combined with raw $CsPbBr_3$ nanocrystals (NCs) [28]. However, the direct deposition for this perovskite film by spraying strategy is rare to date, especially in $CsPb_xMn_{1-x}(Br,Cl)_3$ film material.

Herein, the solution spraying strategy was employed for the direct preparation of $CsPb_xMn_{1-x}(Br,Cl)_3$ film through $MnCl_2$ doping in host $CsPbBr_3$ material for the first time. The soft polyethylene terephthalate (PET) material was used as the substrate. It is well known that the flexible substrate features distinguished plasticity and tailorability, which is favorable to widen the application of prepared $CsPb_xMn_{1-x}(Br,Cl)_3$ material such as curved displaying or wearable devices [29]. In the current work, the influences of $MnCl_2$ doping on the material properties including photoluminescence, structure, morphology, chemical composition, carrier decay lifetime, etc., were investigated in detail. Moreover, the fabrication mechanism of the proposed spraying approach was also analyzed. This work aims to provide a new possibility for the facile preparation of Mn-doping $CsPbX_3$ film material.

2. Experimental Details

2.1. Preparation of $CsPbBr_3$ and $CsPb_xMn_{1-x}(Br,Cl)_3$ Thin Films

Typically, the precursors were prepared by 0.2 mmol CsBr (cesium bromide, 99%, AR), 0.2 mmol $PbBr_2$ (lead bromide, 99%, AR), 40 ul EAC (ethyl acetate, 90%, AR), 40 ul OLA (oleylamine, 70%, AR) and 10 mL DMSO (Dimethyl sulfoxide, 90%) were successively added into the beaker with stirring until reactants were dissolved sufficiently. Then, the transparent solution was poured into spraying devices, and sprayed onto flexible PET substrate at 110 °C within 60 s to obtain the expected sample. Concerning to the fabrication of $CsPb_xMn_{1-x}(Br,Cl)_3$ films, $MnCl_2$ was introduced to partially substitute $PbBr_2$. For $MnCl_2$ (manganese chloride, 99%, AR) doping, the ratio of $PbBr_2$ and $MnCl_2$ was set as 3:1, 3:2 and 1:1, and other experimental conditions were the same as the preparation of $CsPbBr_3$ film. All operations are carried out in the atmosphere. In addition, CsBr and DMSO were provided by Shanghai Titan Scientific Co., Ltd. (Shanghai, China). $PbBr_2$, EAC, OLA and $MnCl_2$ were purchased from Shanghai Aladdin Biochemical Technology Co., Ltd. (Shanghai, China).

2.2. Characterizations for the As-Obtained Samples

The film's surface morphology was measured by scanning electron microscopy (SEM, Quanta 200, FEI, Eindhoven, The Netherlands). The crystalline structure was characterized by X-ray diffraction (XRD, Ultima IV, Rigaku, Tokyo, Japan). An Ultraviolet-Visible-Infrared

spectrophotometer (UV-vis-IR, UH 4150, Hitachi, Tokyo, Japan) was used to record the absorption spectra of the prepared films. The PL properties were measured by fluorescence spectrophotometer (FS5, Edinburgh Instruments, Edinburgh, UK). Energy dispersive X-ray spectroscopy (EDS, Genesis Apollo X, Pittsburgh, PA, USA) and X-ray photoelectron spectroscopy (XPS, Axis Ultra DLD, Kratos, Manchester, UK) were employed for the study of chemical constitution.

3. Results and Discussion

In this work, the preparation diagram was described in Figure 1a. For $CsPbBr_3$ fabrication, all reactants were sufficiently dissolved in DMSO solvent to prepare the precursor solution. In this solution, the mental ions Cs^+, Pb^{2+} dispersed homogeneously and freely. Halide ions Br^- were released from mental halides of CsBr and $PbBr_2$, then acted with OLA to form Br-OLA complexes. During the spraying process, the DMSO solvent was evaporated by the heating treatment. Br^- anions were separated from Br-OLA complexes and combined with Cs^+, Pb^{2+} cations to form the expected $CsPbBr_3$ products. Meanwhile, these $CsPbBr_3$ products may be encapsulated and passivated by OLA molecules as suggested by previous works [30]. For $CsPb_xMn_{1-x}X_3$ film fabrication, Mn^{2+} replaced part of Pb^{2+} (as shown in Figure 1b) and Cl^- exchanged with part Br^- after $MnCl_2$ adding in the precursor solution. Here, the partial substitution of Pb^{2+} by Mn^{2+} was driven by the halide exchange process of Br-to-Cl. During the Br-to-Cl exchange, the rigid octahedron structure of $PbBr_6^{4-}$ would be opened up, and then the Mn^{2+} would be incorporated into this structure to replace Pb^{2+}. The above halide exchange driven cation exchange process has also been demonstrated by early studies [31].

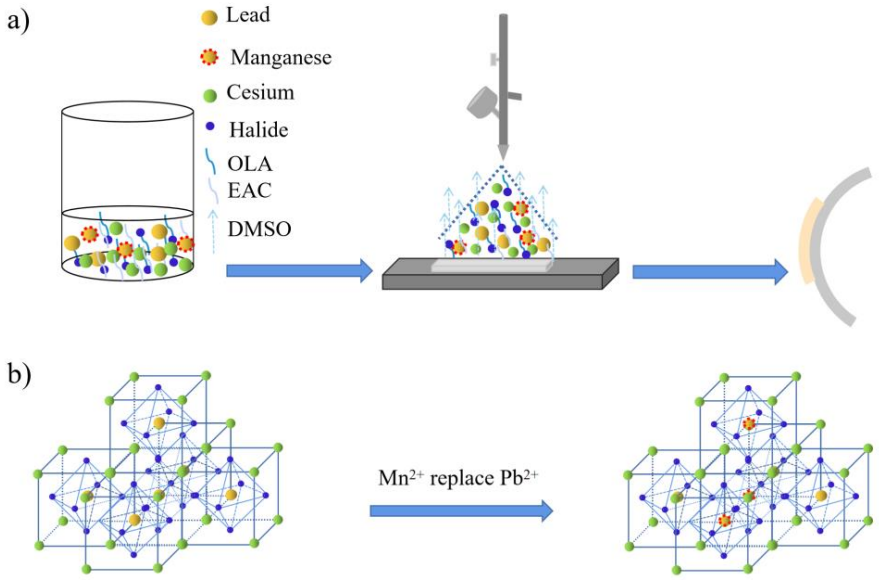

Figure 1. (**a**) The schematic diagram of solution spraying process; (**b**) Mn^{2+} replaced part of Pb^{2+}.

The PL spectra of $CsPbBr_3$ and $CsPb_xMn_{1-x}(Br,Cl)_3$ films were shown in Figure 2a. For $CsPbBr_3$ film, an emission band centered at 515 nm is observed, while the peaks at 450/470 nm could be attributed to EAC. When doped with $MnCl_2$, two peaks at around 509/616 nm were observed. It was found that the main peak of 515 nm in pure $CsPbBr_3$ film gradually blue-shifted to 505 nm with the ratio of $PbBr_2$:$MnCl_2$ increasing from 3:1 to 1:1. This may be caused by the band gap varying, which resulted from the increasing Br-to-Cl exchanging after $MnCl_2$ incorporation [22,32]. The peak locating at 616 nm was derived from the energy transferring of $^4T_1 \rightarrow {}^6A_1$ caused by Mn substitution for Pb in $CsPb_xMn_{1-x}(Br,Cl)_3$ material. In $CsPb_xMn_{1-x}(Br,Cl)_3$, after band to band optical excitation, the energy is transferred from the main material to the Mn^{2+} excited state [33]. In addition, the Mn^{2+} emission slightly red-shifted from 616 nm to 619 nm as the Mn ratio increased.

This may be caused by the lattice contraction induced modification of Mn^{2+} ligand-field and the Mn^{2+} reabsorption/emission effect as suggested [22]. As observed, the PLQY values of the samples, prepared with different $PbBr_2$: $MnCl_2$ ratios of 3:0, 3:1, 3:2, 1:1, were 15.68%, 1.26%, 3.85% and 3.09%, respectively. It was found that the PLQY of $MnCl_2$ doped samples displayed a downward trend when the $PbBr_2$: $MnCl_2$ ratio was over 3:2. This may be caused by a quenching effect due to excessive Mn. Figure 2b depicted the Commission Internationale de I'Eclairage (CIE) color space coordinates of $CsPbBr_3$ and $CsPb_xMn_{1-x}(Br,Cl)_3$ films. For the $CsPbBr_3$ sample, the CIE was (0.2329, 0.5913) and showed green light under 365 nm UV excitation. For the $CsPb_xMn_{1-x}(Br,Cl)_3$ sample, the corresponding CIE of different Pb/Mn ratios (3:1, 3:2, 1:1) were (0.2891, 0.3657), (0.3853, 0.3625), and (0.4294, 0.3757), respectively, and the as-prepared samples featured cyan, orange-red, pink-red separately. The cyan color for the sample fabricated under 3:1 Pb/Mn ratio may occur because the emission of main material was dominant while the energy transferring was in a low degree. With the increasing Mn content, the energy transferring was accelerated. This was well suggested by the color changing and the variation of normalized Mn^{2+} emission intensity. Additionally, the color purity was 53.8%, 20.1%, 24.4% and 41.6%, while the color temperature was 7344, 7839, 3749 and 2889 K, for 3:0, 3:1, 3:2 and 1:1 Pb/Mn ratio, respectively.

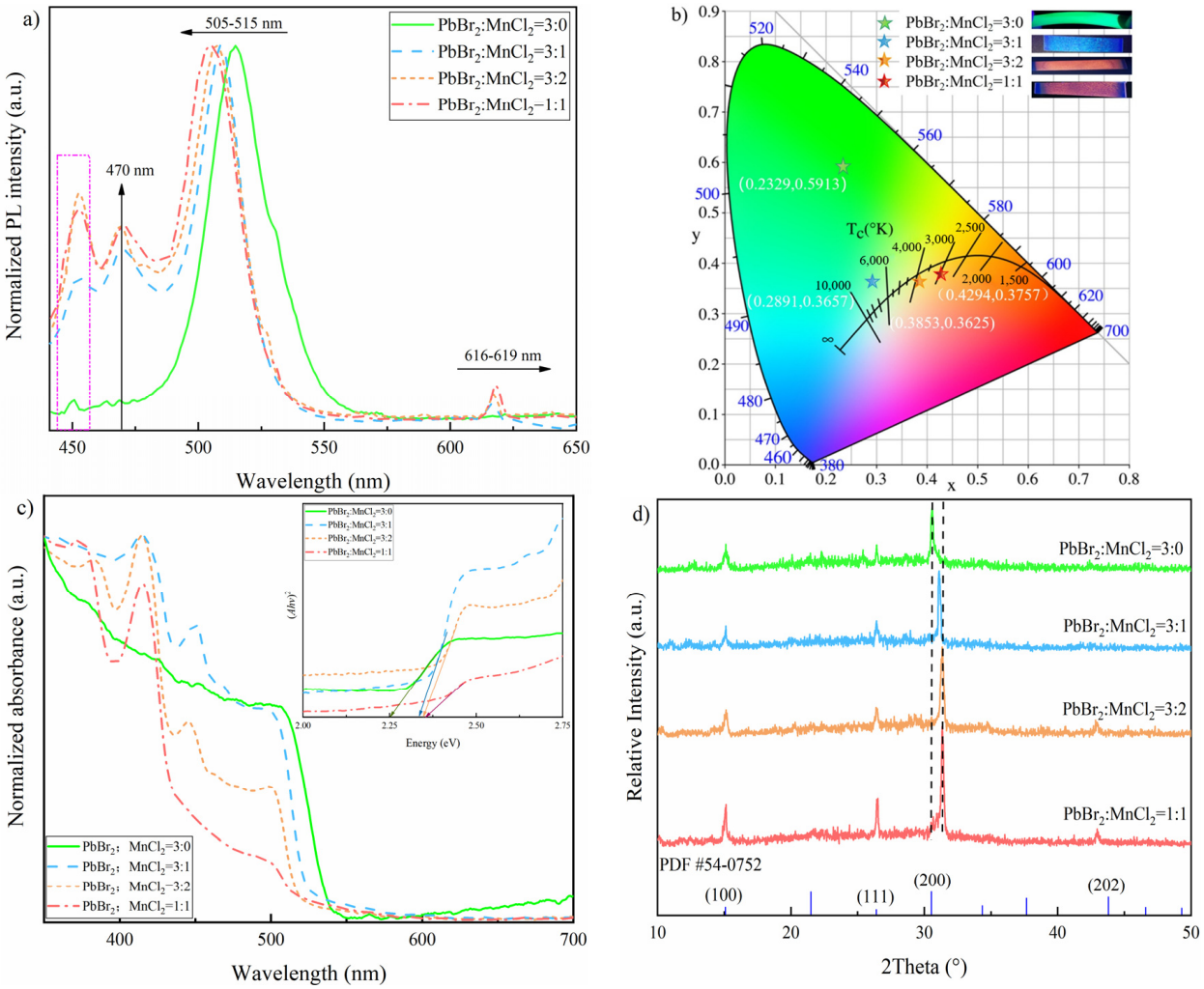

Figure 2. Optical properties of as-obtained samples prepared by different $PbBr_2/MnCl_2$ ratios: (**a**) PL spectra; (**b**) CIE diagram; (**c**) absorption spectra (inset plots of $(Ahv)^2$ vs. (hv)); and (**d**) XRD pattern.

Furthermore, the absorbance spectra of as-obtained samples were determined by UV-vis spectrophotometer and displayed in Figure 2c. As observed, all samples had absorption edges around 510 nm, which was attributed to main materials $CsPb(Br/Cl)_3$. Additionally, this edge bule-shifted gradually, with the increasing Cl^-. The bandgap energy *Eg* of these samples were calculated by extrapolating the straight line of $(Ahv)^2$ vs. (hv) plots displayed in the inset of Figure 2c. Here, A is absorbance, *h* is Planck's constant, *v* is frequency. As observed, the *Eg* values for Mn-doped $CsPbBr_3$ films (with the ratio of $PbBr_2$:$MnCl_2$ 3:0, 3:1, 3:2, 1:1) were 2.25, 2.33, 2.34 and 2.35 eV, separately. The crystal structure of prepared films was determined by XRD treatment as shown in Figure 2d. Regarding to the undoped sample, there were three peaks, locating around at 15.02°, 26.39°, and 30.56°, could be attributed to the (100), (111), and (200) planes of cubic $CsPbBr_3$ (JCPDS 54-0752). This indicated the undoped sample was in pure perovskite phase. It was found that the diffraction peak of (202) plane gradually appeared at around 42.80° with $MnCl_2$ doping increasing. Interestingly, the diffraction peak of (200) plane gradually shifted toward to higher angles as $MnCl_2$ doping increased. As suggested by early studies [22], this was caused by the lattice contraction after the smaller Mn^{2+} (0.97 Å) and Cl^- incorporation into the lattice to separately replace Pb^{2+} (1.33 Å) and Br^-. This is also confirmed by the changing of crystal size of prepared films. As calculated based on (200) plane by Scherrer formula, the crystal sizes corresponding to the different ratios of $PbBr_2$:$MnCl_2$ (3:0, 3:1, 3:2, 1:1) were 22.03, 21.31, 20.86, and 19.96 nm, respectively, which presented a downward trend.

The surface morphologies of the samples prepared in 3:0, 3:1, 3:2 and 1:1 $PbBr_2$:$MnCl_2$ ratios were shown in Figure 3a–d, respectively. It was found that the undoped sample was in bulk-shape, and was dense and compact. This was benefitted from the Br-rich state as suggested by previous studies [34]. A few particles also appeared on the surface. As suggested by previous studies [30], the bulk-shaped or particle-shaped products were composed of agglomerated NCs by soft agglomeration of electrostatic force or Van der Waals force, especially in the presence of OLA. Interestingly, the dense and compact state of as-fabricated samples deteriorated as the $MnCl_2$ ratio increased. More and more particles appeared as well as the pins. This was because Br was partially replaced by Cl to change the Br-rich state after $MnCl_2$ doping. Thus, the morphology featured a deterioration trend with more Cl incorporating into the prepared film samples. Furthermore, the EDS mappings were also described in Figure 3a–d to determine the chemical composition of as-obtained samples prepared with different $PbBr_2$:$MnCl_2$ ratios. As observed, all elements including Cs, Pb/Mn, Br/Cl dispersed homogeneously on the sample surfaces. Concerning the Mn atom percent in prepared samples, the value increased from 0 to 10.73% with the Pb/Mn ratio varying from 3:0 to 1:1. The actual Pb/Mn ratios were 3:0, 2.8:1, 3.1:2 and 0.93:1, which were close to the expected values of 3:0, 3:1, 3:2 and 1:1. This indicated Pb was successfully substituted by Mn in host material as expected. In addition, the Cs:(Pb+Mn):(Cl+Br) ratio of fabricated samples was close to the stoichiometric value 1:1:3.

XPS survey was employed to further investigate the composition of as-prepared samples. As observed in Figure 4a, the orbital peaks of Mn 2p and Cl 2p appeared as expected in $MnCl_2$ dopped sample comparing to the pure $CsPbBr_3$ film. Cs, Pb and Br all had two split peaks locating at around 737.78 and 723.81 eV, 142.34 and 137.45 eV, and 68.45 and 67.56 eV, which were assigned to Cs $3d_{3/2}$ and Cs $3d_{5/2}$, Pb $4f_{5/2}$ and Pb $4f_{7/2}$, and Br $3d_{3/2}$ and Br $3d_{5/2}$ electronic levels, respectively, as displayed in Figure 4b–d [35]. Note that these peaks all slightly shifted to high binding energy as $MnCl_2$ increased, especially for Pb 4f. This may be caused by the coordination bonding of Cs-Cl, Pb-Cl and Mn-Br on the surface of host material. This was favorable for the stability improvement of Cs 3d, Pb 4f and Br 3d. In addition, the obvious red-shifting of Pb 4f may also be a result from the changing of chemical environment and electron density after Mn doping as suggested by previous work [32,36]. Figure 4e showed two characteristic peaks located at 641.63 eV and 650.31 eV corresponding to Mn $2p_{3/2}$ and Mn $2p_{1/2}$, respectively. This indicated Mn was in divalent state, and also suggested Pb was successfully substituted by Mn as expected [35].

Similar to Cs and Pb, the binding energy of Mn $2p_{1/2}$ also slightly varied to a higher value as $MnCl_2$ doping increased. For Cl, there were two peaks that appeared at 197.25 and 198.95 eV, as observed in Figure 4f.

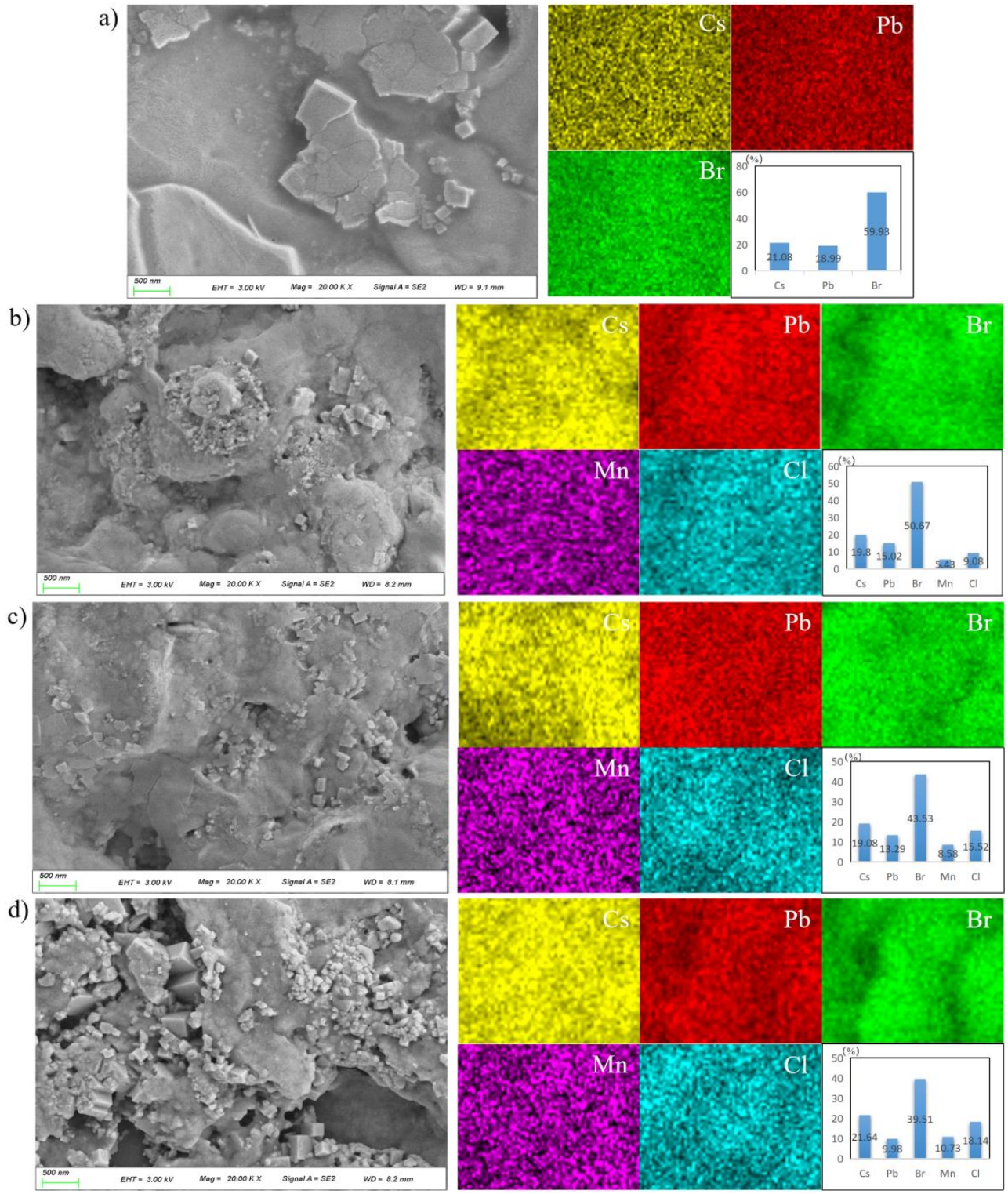

Figure 3. Morphologies and EDS mappings of the samples prepared by different $PbBr_2/MnCl_2$ ratios: (**a**) 3:0; (**b**) 3:1; (**c**) 3:2; (**d**) 1:1.

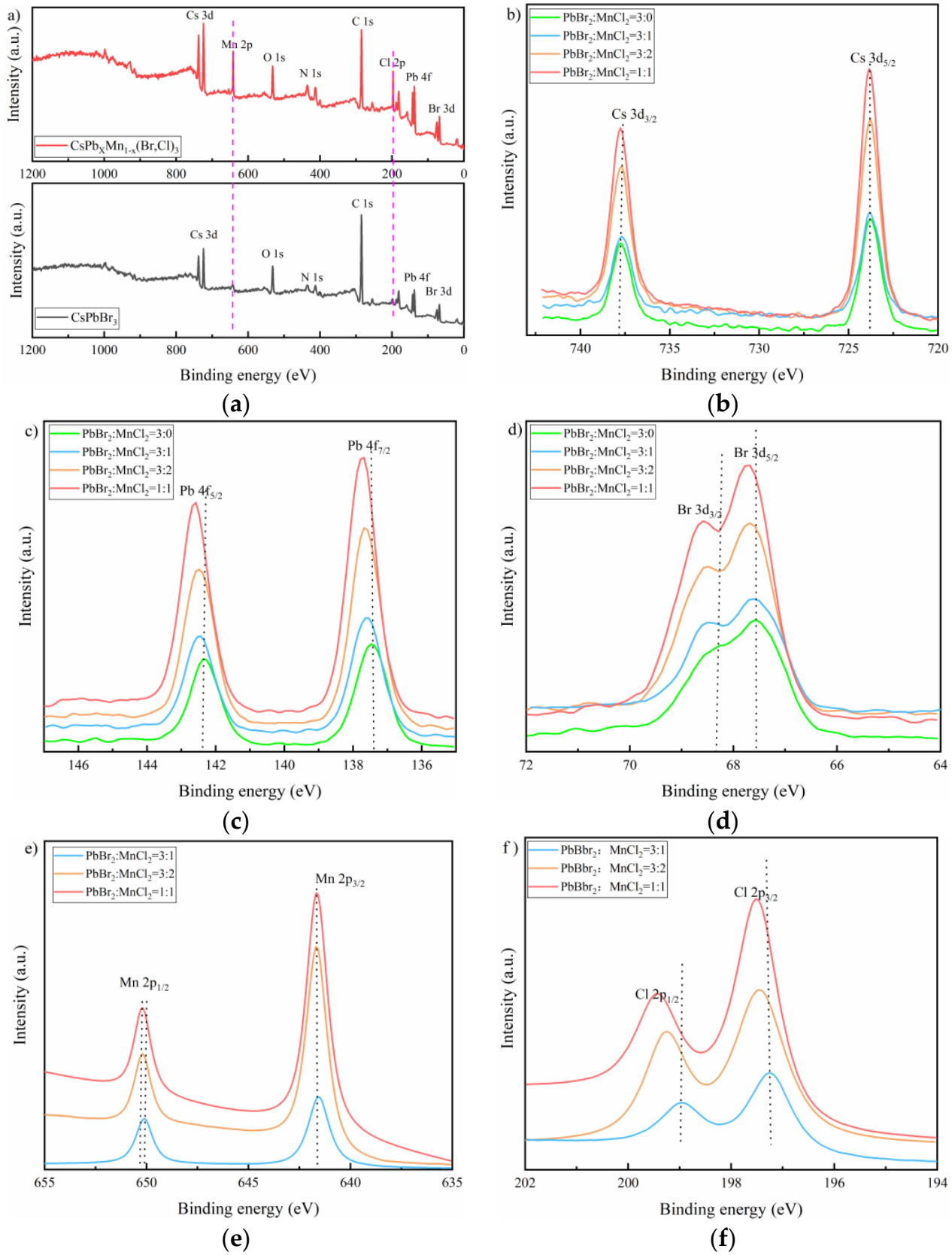

Figure 4. (**a**) XPS survey spectra of Mn-doped and undoped samples; the combining energy of different elements: (**b**) Cs 3d, (**c**) Pb 4f, (**d**) Br 3d, (**e**) Mn 2p, and (**f**) Cl 2p.

Figure 5 displayed the normalized time-resolved PL decay curves of as-prepared films. The curves were fitted by a bi-exponential function as shown in Equation (1):

$$y = A_0 + A_1 \exp\left(-\frac{t}{\tau_1}\right) + A_2 \exp\left(-\frac{t}{\tau_2}\right) \quad (1)$$

$$\tau_{ave} = \left(A_1\tau_1^2 + A_2\tau_2^2\right)/(A_1\tau_1 + A_2\tau_2) \quad (2)$$

where, τ_1, τ_2 are short-lived and long-lived lifetime originating from exciton radiative recombination and the trap-assisted nonradiative recombination, respectively. A_1 and A_2 are the corresponding occupied percent of τ_1 and τ_2, respectively. A_0 is a constant, the average lifetime τ_{ave} is calculated by Equation (2). As observed, the values of τ_1, τ_2 and τ_{ave} all featured a downward trend as $MnCl_2$ doping increased. It is worth mentioning that the value of τ_1 decreased from 1.94 ns to 1.14 ns, which may be derived from the bandgap increasing caused by Br-to-Cl anion exchange [22]. Moreover, the occupied percent of τ_1 was increased from 35.70% to 49.00% which meant a higher ratio of radiative to nonradiative recombination. Above indicated a better exciton emission and less defect-related transition, as suggested by previous studies [30].

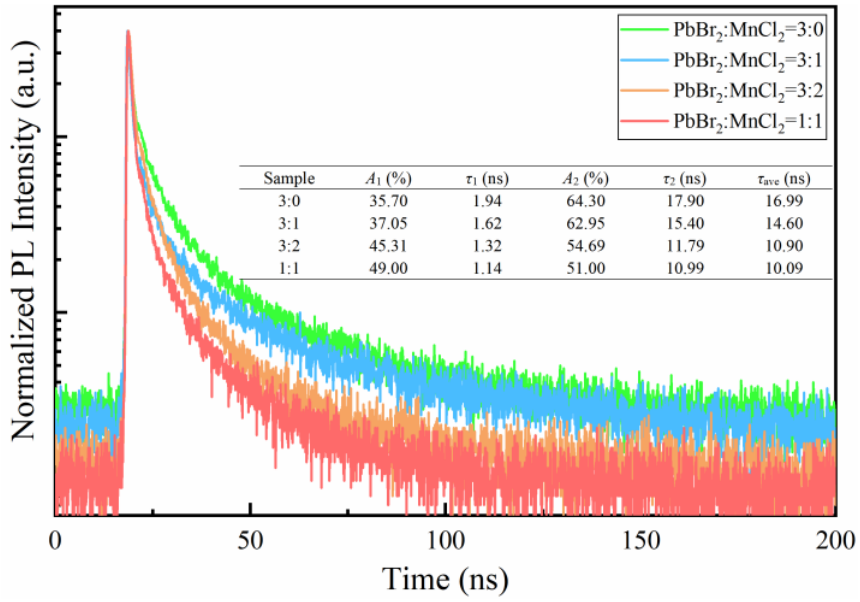

Sample	A_1 (%)	τ_1 (ns)	A_2 (%)	τ_2 (ns)	τ_{ave} (ns)
3:0	35.70	1.94	64.30	17.90	16.99
3:1	37.05	1.62	62.95	15.40	14.60
3:2	45.31	1.32	54.69	11.79	10.90
1:1	49.00	1.14	51.00	10.99	10.09

Figure 5. Time-resolved PL decay curves of the samples prepared by different $PbBr_2/MnCl_2$ ratios.

4. Conclusions

In conclusion, a $CsPb_xMn_{1-x}(Br,Cl)_3$ film was successfully prepared by facile solution spraying approach with flexible PET substrate through $MnCl_2$ doping in host $CsPbBr_3$ material. As the results showed, the green emission in $CsPbBr_3$ film gradually transferred to be cyan, orange-red, and pink-red as $MnCl_2$ increased, which was derived from the energy transferring between host material and Mn^{2+} excited state. It was found that the dense and compact film was varied to be a coexisting state of bulk and nanoparticles products with the $MnCl_2$ increasing in doped material. The EDS mapping displayed that all chemical dispersed uniformly on the film surface, and Pb was successfully substituted by Mn as expected, which was further confirmed by XPS investigation. Moreover, with $MnCl_2$ doping rising, the combining energy of Cs, Pb, and Mn featured a red-shifting variation which may be caused by the formation of Cs-Cl, Pb-Cl and Mn-Br coordination bonding. Time-resolved PL decay study indicated the weight of short-lifetime presented an upward trend as doping increased, which suggested a better exciton emission and less defect-related transition.

Author Contributions: Conceptualization, Y.S. and J.C.; methodology, Y.S., J.C. and C.Z.; formal analysis, J.C., Y.S. and J.K.; investigation, Y.S., Y.Y., X.P. and R.H.; writing—original draft preparation, Y.S.; writing—review and editing, Y.S., J.C. and F.W.; supervision, F.W.; project administration, J.C. and J.W.; funding acquisition, J.C., Y.J. and J.Y. All authors have read and agreed to the published version of the manuscript.

Funding: The project was sponsored by Shanghai Sailing Program, China (No.18YF1422500, No. 20YF1447600), and Collaborative innovation project of Shanghai Institute of Technology (No. XTCX2020-12).

Institutional Review Board Statement: Not applicable.

Informed Consent Statement: Not applicable.

Data Availability Statement: Not applicable.

Conflicts of Interest: The authors declare no conflict of interest.

References

1. Gualdron-Reyes, A.F.; Yoon, S.J.; Barea, E.M.; Agouram, S.; Munoz-Sanjose, V.; Melendez, A.M.; Nino-Gomez, M.E.; Mora-Sero, I. Controlling the phase segregation in mixed halide perovskites through nanocrystal size. *ACS Energy Lett.* **2019**, *4*, 54–62. [CrossRef] [PubMed]
2. Selopal, G.S.; Zhao, H.G.; Wang, Z.M.; Rosei, F. Core/Shell Quantum Dots Solar Cells. *Adv. Funct. Mater.* **2020**, *30*, 1908762. [CrossRef]
3. Xing, G.; Mathews, N.; Lim, S.S.; Yantara, N.; Liu, X.; Sabba, D.; Grtzel, M.; Mhaisalkar, S.; Sum, T.C. Low-temperature solution-processed wavelength-tunable perovskites for lasing. *Nat. Mater.* **2014**, *13*, 476–480. [CrossRef]
4. Park, Y.S.; Bae, W.K.; Baker, T.; Lim, J.; Klimov, V.I. Effect of auger recombination on lasing in heterostructured quantum dots with engineered core/shell interfaces. *Nano Lett.* **2015**, *15*, 7319–7328. [CrossRef]
5. Andrés Fabian, G.R.; Jhonatan, R.P.; Eliseo, A.G.; Jorge, R.P.; Rogelio, O.; Sofia, M.; Joon, Y.; Juan, T.; Franklin, J.; Said, A.; et al. Unravelling the photocatalytic behavior of all-inorganic mixed halide perovskites: The role of surface chemical states. *ACS Appl. Mater. Interfaces* **2019**, *12*, 914–924.
6. Suarez, I.; Juarez-Perez, E.J.; Bisquert, J.; Mora-Sero, I.; Martinez-Pastor, J.P. Polymer/perovskite amplifying waveguides for aactive hybrid silicon photonics. *Adv. Mater.* **2015**, *27*, 6157–6162. [CrossRef] [PubMed]
7. Manav, R.K.; Smaranika, R.; Saikat, B. State of the art and prospects of metal halide perovskite core@shell nanocrystals and nanocomposites. *Mater. Today Chem.* **2021**, *20*, 100424.
8. Abhishek, S.; Ramya, C.; Vikash, K.R.; Mir, I.; Arindam, C.; Angshuman, N. Colloidal $CsPbBr_3$ perovskite nanocrystals: Luminescence beyond traditional quantum dots. *Angew. Chem.* **2015**, *127*, 15644–15648.
9. Green, M.A.; Ho-Baillie, A.; Snaith, H.J. The emergence of perovskite solar cells. *Nat. Photonics* **2014**, *8*, 506–514. [CrossRef]
10. Protesescu, L.; Yakunin, S.; Bodnarchuk, M.I.; Krieg, F.; Caputo, R.; Hendon, C.H.; Yang, R.X.; Walsh, A.; Kovalenko, M.V. Nanocrystals of cesium lead halide perovskites ($CsPbX_{(3)}$, X = Cl, Br, and I): Novel optoelectronic materials showing bright emission with wide color gamut. *Nano Lett.* **2015**, *15*, 3692–3696. [CrossRef]
11. Zhang, Y.; Liu, J.; Wang, Z.; Xue, Y.; Ou, Q.; Polavarapu, L.; Zheng, J.; Qi, X.; Bao, Q. Synthesis, properties, and optical applications of low-dimensional perovskites. *Chem. Commun.* **2016**, *52*, 13637–13655. [CrossRef]
12. Babayigit, A.; Ethirajan, A.; Muller, M.; Conings, B. Toxicity of organometal halide perovskite solar cells. *Nat. Mater.* **2016**, *15*, 247–251. [CrossRef] [PubMed]
13. Stam, W.V.D.; Geuchies, J.J.; Altantzis, T.; Bos, K.H.V.D.; Meeldijk, J.D.; Aert, S.V.; Bals, S.; Vanmaekelbergh, D. Highly emissive divalent-ion-doped colloidal $CsPb_{1-x}M_xBr_3$ perovskite nanocrystals through cation exchange. *J. Am. Chem. Soc.* **2017**, *139*, 4087–4097. [CrossRef]
14. Guo, Y.; Su, J.; Wang, L.; Lin, Z.; Hao, Y.; Chang, J. Improved doping and optoelectronic properties of Zn-doped $CsPbBr_3$ perovskite through Mn codoping approach. *J. Phys. Chem. Lett.* **2021**, *12*, 3393–3400. [CrossRef]
15. Liu, W.; Lin, Q.; Li, H.; Wu, K.; Klimov, V.I. Mn^{2+}-doped lead halide perovskite nanocrystals with dual-color emission controlled by halide content. *J. Am. Chem. Soc.* **2016**, *138*, 14954–14961. [CrossRef] [PubMed]
16. Zou, S.; Liu, Y.; Li, J.; Liu, C.; Feng, R.; Jiang, F.; Li, Y.; Song, J.; Zeng, H.; Hong, M.; et al. Stabilizing cesium lead halide perovskite lattice through Mn (II)-substitution for air-stable light-emitting diodes. *J. Am. Chem. Soc.* **2017**, *139*, 11443–11450. [CrossRef] [PubMed]
17. Parobek, D.; Roman, B.J.; Dong, Y.; Jin, H.; Lee, E.; Sheldon, M.; Son, D.H. Exciton-to-dopant energy transfer in Mn-doped cesium lead halide perovskite nanocrystals. *Nano Lett.* **2016**, *16*, 7376–7380. [CrossRef] [PubMed]
18. Akkerman, Q.A.; Meggiolaro, D.; Dang, Z.; Angelis, F.D.; Manna, L. Fluorescent alloy $CsPb_xMn_{1-x}I_3$ perovskite nanocrystals with high structural and optical stability. *ACS Energy Lett.* **2017**, *2*, 2183–2186. [CrossRef]
19. Szeremeta, J.; Antoniak, M.A.; Wawrzynczyk, D.; Nyk, M.; Samoc, M. The two-photon absorption cross-section studies of $CsPbX_3$ (X = I, Br, Cl) nanocrystals. *Nanomaterials* **2020**, *10*, 1054. [CrossRef] [PubMed]

20. Li, Z.; Song, C.; Rao, L.; Lu, H.; Yan, C.; Cao, K.; Ding, X.; Yu, B.; Tang, Y. Synthesis of highly photoluminescent all-inorganic $CsPbX_3$ nanocrystals via interfacial anion exchange reactions. *Nanomaterials* **2019**, *9*, 1296. [CrossRef] [PubMed]
21. Zhu, J.; Yang, X.; Zhu, Y.; Wang, Y.; Cai, J.; Shen, J.; Sun, L.; Li, C. Room temperature synthesis of Mn-doped cesium lead halide quantum dots with high Mn substitution ratio. *J. Phys. Chem. Lett.* **2017**, *8*, 4167–4171. [CrossRef] [PubMed]
22. Chen, D.; Fang, G.; Chen, X.; Lei, L.; Zhong, J.; Mao, Q.; Zhou, S.; Li, J. Mn-doped $CsPbCl_3$ perovskite nanocrystals: Solvothermal synthesis, dual-color luminescence and improved stability. *J. Mater. Chem. C* **2018**, *6*, 8990–8998. [CrossRef]
23. Mei, S.; Yang, B.; Wei, X.; Dai, H.; Chen, Z.; Cui, Z.; Zhang, G.; Xie, F.; Zhang, W.; Guo, R. Facile synthesis and optical properties of $CsPbX_3$/ZIF-8 composites for wide-color-gamut display. *Nanomaterials* **2019**, *9*, 832. [CrossRef] [PubMed]
24. Skorupska, E.; Jeziorna, A.; Potrzebowski, M.J. Thermal solvent-free method of loading of pharmaceutical cocrystals into the pores of silica particles: A case of naproxen/picolinamide cocrystal. *J. Mater. Chem. C* **2016**, *120*, 13169–13180. [CrossRef]
25. Wang, Y.; Han, S.; Hao, L.; He, L.; Wei, G.; Wu, M.; Wang, H.; Liu, Y.; Chen, D. New type of neutron image scintillator based on $H_3{}^{10}BO_3$/ZnS(Ag). *Phys. Procedia* **2013**, *43*, 216–222. [CrossRef]
26. Hadi, Z.L.; Essa, M.S.; Chiad, B.T. Ternary Cu_2SnS_3 thin films deposited by fully controlled system of spray pyrolysis. *J. Phys. Conf. Ser.* **2019**, *1234*, 012041. [CrossRef]
27. Wang, F.; Peng, X.; Sun, Y.; Chen, J.; Ju, J.; Jin, Y.; Zhang, C.; Kong, J.; Yang, J.; Chen, Q.; et al. Influences of rapid thermal annealing on Cu_2ZnSnS_4 thin film fabricated by spraying approach. *J. Mater. Sci. Mater. Electron.* **2021**, *32*, 7153–7161. [CrossRef]
28. Yang, Z.; Wang, M.; Li, J.; Dou, J.; Qiu, H.; Shao, J. Spray-coated $CsPbBr_3$ quantum dot Films for perovskite photodiodes. *ACS Appl. Mater. Interfaces* **2018**, *10*, 26387–26395. [CrossRef] [PubMed]
29. Nie, J.; Zhu, L.; Zhai, W.; Berbille, A.; Li, L.; Wang, Z. Flexible piezoelectric nanogenerators based on P(VDF-TrFE)/$CsPbBr_3$ quantum dot composite films. *ACS Appl. Electron. Mater.* **2021**, *3*, 2136–2144. [CrossRef]
30. Wang, F.; Peng, X.; Wang, C.; Dong, H.; Sun, Y.; Kong, J.; Zhang, C.; Chen, J.; Li, L.; Xu, J. Synthesis of $CsPbBr_3$ and $CsPbBr_XI_{(3-X)}$ films by spray-coating technique. *ECS J. Solid State SC* **2020**, *9*, 126007. [CrossRef]
31. Chen, D.; Zhou, S.; Fang, G.; Chen, X.; Zhong, J. Fast room-temperature cation exchange synthesis of Mn-doped $CsPbCl_3$ nanocrystals driven by dynamic halogen exchange. *ACS Appl. Mater. Interfaces* **2018**, *10*, 39872–39878. [CrossRef]
32. Xu, K.; Vickers, E.T.; Luo, B.; Allen, A.C.; Chen, E.; Roseman, G.; Wang, Q.; Kliger, D.S.; Millhauser, G.L.; Yang, W.; et al. First synthesis of Mn-doped cesium lead bromide perovskite magic sized clusters at room temperature. *J. Phys. Chem. Lett.* **2020**, *11*, 1162–1169. [CrossRef] [PubMed]
33. Pradhan, N.; Peng, X. Efficient and color-tunable Mn-doped ZnSe nanocrystal emitters: Control of optical performance via greener synthetic chemistry. *J. Am. Chem. Soc.* **2007**, *129*, 3339–3347. [CrossRef] [PubMed]
34. Wang, Z.; Luo, A.; Zhao, C.; Guo, Q.; Wang, Y.; Wang, F.; Bian, X.; Alsaedi, A.; Hayat, T.; Tan, Z. Efficient and stable pure green all-inorganic perovskite $CsPbBr_3$ light-emitting diodes with a solution-processed NiO_x interlayer. *J. Phys. Chem. C* **2017**, *121*, 28132–28138. [CrossRef]
35. He, M.; Cheng, Y.; Shen, L.; Zhang, H.; Shen, C.; Xiang, W.; Liang, X. Doping manganese into $CsPb(Cl/Br)_3$ quantum dots glasses: Dual-color emission and super thermal stability. *J. Am. Ceram. Soc.* **2019**, *102*, 1090–1100. [CrossRef]
36. Liu, M.; Zhong, G.; Yin, Y.; Miao, J.; Li, K.; Wang, C.; Xu, X.; Shen, C.; Meng, H. Aluminum-doped cesium lead bromide perovskite nanocrystals with stable blue photoluminescence used for display backlight. *Adv. Sci.* **2017**, *4*, 1700335. [CrossRef] [PubMed]